

Optimized Bearing and Interlayer Friction in Multiwalled Carbon Nanotubes

Wanlin Guo^{1,2} and Huajian Gao²

Abstract: A systematic investigation is performed on energy dissipation related interaction force associated with interlayer motion of sliding, rotation and telescoping between any two possible neighboring carbon nanotubes. In particular, we analyze the interlayer corrugation energy and sliding, rotation and telescoping resistance force associated with the Lennard-Jones potential as well as a registry-dependent graphitic potential. It is found that the interlayer resistance associated with both of these potentials can vary with the morphology, length and diameter of the two tubes. Energy dissipation related fluctuation of the resistant force can be as low as 10^{-18} N/atom between the most optimistic tube pairs, but can be as large as 10^{-11} N/atom in the widely investigated zigzag/zigzag orientations. In most cases, the fluctuation of interlayer sliding resistance force increases with the tube length in a commensurate pair of tubes, but can remain unchanged in an incommensurate pair. These findings may be significant for the design of nanotube-based devices.

keyword: Friction, energy dissipation, molecular mechanics, commensuration, multi-walled carbon nanotube.

1 Introduction

The ultra-low interlayer corrugation and friction force in multiwalled carbon nanotubes (MWCNTs) have been shown both theoretically [Kolmogorov and Crespi (2000); Damnjanovic, Milosevic, Vukovic and Sredanovic (1999); Hirano, Shinjo, Kaneko and Murata (1997)] and experimentally [Yu, Yakobson and Ruoff (2000); Cumings and Zettl (2000)]. Combining this property and other exceptional mechanical [Robertson, Brenner and Mintmire (1992); Treacy, Ebbesen and

Gibson (1996); Wong, Sheehan and Lieber (1997); Yu, Lourie, Dyer, Moloni, Kelly and Ruoff (2000); Collins, Arnold and Avouris (2001)] and electronic properties [Dai, Wong and Lieber (1996); Guo and Guo (2003); Tans, Verschueren and Dekker (1998); Martel, Schmidt, Shea, Hertel and Avouris (1998); Collins, Arnold and Avouris (2001)], MWCNTs have been identified as the top candidates for nano-electromechanical systems [Postma, Teepen, Yao, Grifoni and Dekker (2001); Rueckes, Kim, Joselevich, Tseng, Cheung and Lieber (2000); de Heer, Bacsá, Chatelain, Gerfin, Humphrey-Baker, Forro and Ugarte (1995); Forro, L. (1995); Zheng and Jiang (2002)]. Many such properties, including the interlayer friction, are strongly dependent on the structural anisotropy of MWCNTs [Dai (2002); Roche, Triozon, Rubio and Mayou (2001); Hamada, Sawada, Oshiyama (1992); Odom, Huang, Kim and Lieber (1998); Shyu and Lin (2000)] and need to be more thoroughly investigated.

Recently, Cumings and Zettl (2000) demonstrated that the cyclic interlayer sliding is wear-free; the force to extract a core tube out of an outer housing tube is constant; the friction force is estimated to be lower than 10^{-14} N/atom, interlayer sliding takes place between the same two nanotube shells which apparently offer the least resistance to interlayer motion; and there is no multiple telescoping (i.e. simultaneous sliding among different layers). This self-selection and self-optimization property of MWCNTs is very intriguing and could have great potential for applications in nano-electromechanical devices.

The interaction between two layers of MWCNTs is dominated by the long range van der Waals force. Significant effort has been made to understand van der Waals interaction between two graphite layers or CNT shells [Tanaka, Aoki, Ago, Yamare and Okahara (1997); Benedict, Chopra, Cohen, Zettl, Louie and Crespi (1998); Paulson, Helser, Nardelli, Taylor II, Falvo, Superfine and Washburn (2000); Brenner, Shenderova, Areshkin, Schall and

¹Institute of Nano Science, Nanjing University of Aeronautics and Astronautics, Nanjing, 210016, China.

E-mail: wlguo@nuaa.edu.cn.

²Max-Planck Institute for Metals Research, Heisenbergstrasse 3, D-70569 Stuttgart, Germany.

Frankland (2002); Shen and Atluri (2004)]. However, it is still very difficult to model van der Waals forces by quantum mechanics [Girifalco and Hodak (2002)], and most studies of interlayer interaction have been based on the Lennard-Jones (L-J) potential. Kolmogorov and Crespi (2000) (K-C) proposed a new registry dependent two body graphitic potential to model the effects of the tube morphology and atom number on sliding interlayer corrugation. It was shown that for a variety of axially incommensurate tube pairs, the interlayer sliding corrugation can be extremely low.

Using static continuous models on excess van der Waals interlayer interaction energy of MWCNTs, Zheng and collaborators [Zheng and Jiang (2002); Zheng, Liu and Jiang (2002)] have proposed the possibility to create nanooscillators of operating frequency up to several gigahertz. Recent molecular dynamical simulations demonstrate that sustained oscillations are possible in these devices [Legoas, Coluci, Braga, Coura, Dantas and Galvao (2003)]. However, to create a physical set up of these devices the resistant force to the motion and energy dissipation rate have to be considered [Guo, Guo, Gao, Zheng and Zhong (2003); Rivera, McCabe and Cummings (2003)]. The energy dissipation related interlayer resistance force may play a key role in many other nanodevices such as nanobearings, nanoswitches and constant force nanosprings as well.

In this paper, we conduct a systematic investigation of the resistance forces associated with interlayer motion in MWCNTs using both the L-J potential and K-C potential. Energy corrugation and the resistance forces associated with interlayer motion including sliding, rotating and telescoping between an arbitrarily chosen pair of neighboring tube shells are found to be closely dependent on the commensuration of the tube pair. A thorough comparison of the two interlayer potentials is presented and size effects are also analyzed.

2 Background

Following the notation of White, Robertson and Mintmire (1993), each SWCNT is indexed by a pair of integers (n, m) which define the circumferential direction in graphitic lattice coordinates. For symmetry, we take $n \geq m$ in this study. The SWCNT radius is given by

$$R = \frac{\sqrt{3}a_0}{2\pi} n \sqrt{1+x+x^2} \quad (1)$$

where $x = m/n$ and a_0 is the length of the C-C bond which is taken as 1.42\AA . With this definition, $x=0$ denotes an zigzag and $x=1$ an armchair SWCNT, and $0 < x < 1$ covers all possible orientation. We consider the cases $x \cong 0, 0.2, 0.4, 0.6, 0.8$ and 1.0 in this investigation.

Assuming interlayer sliding within a MWCNT only occurs between two layers with least resistance force [Cumings and Zettl (2000)], we will focus on a two-walled bi-tube system. Subscript "o" denotes the outer shell and "c" the inner core tube. We use x_o/x_c to describe the bi-tube system. For example, the armchair/armchair system is $1/1$, zigzag/zigzag is $0/0$ and zigzag/armchair is $0/1$. The ends of all tubes are open without any terminal group.

For given inner tube radius R_c and fractional index x , the index (n_c, m_c) can be determined from the best approximation to R_c and x . The interlayer distance $\Delta R = R_o - R_c$ in a MWCNT is reported to be about 3.4\AA and may change in the range from 3.354\AA to 3.6\AA in bulk graphite. The index (n_o, m_o) is determined from the conditions $R_o \approx R_c + 3.4\text{\AA}$ and $3.35\text{\AA} < \Delta R < 3.75\text{\AA}$. If there are multiple choices, then one in the range $\Delta R \in [3.35, 3.40]$ and one in the range $\Delta R \in [3.40, 3.75]$ will be selected. In most of the calculation, $R_c \cong 20\text{\AA}$ is selected according to Cumings and Zettl's experiment.

The interlayer potential are described in the appendix and the total interlayer interaction energy is

$$E_{pot} = \sum_{i=1}^{N_c} \sum_{j=1}^{N_o} V(r_{ij}) \quad (2)$$

where i denotes an atom in the inner shell and j an atom in the outer shell, N_c and N_o being the numbers of atoms of the inner and outer shells, respectively. The radius of cut-off for energy calculation is set for 5 times of the C-C bond length.

For rigid tubes, the interlayer sliding and rotational resistance forces can be calculated by

$$F_{slid} = -\frac{\partial E_{pot}}{\partial \xi}; \quad F_{rot} = -\frac{1}{R_c} \frac{\partial E_{pot}}{\partial \theta} \quad (3)$$

Where ξ is the relative sliding displacement and θ the relative angular displacement between the inner and outer shells.

3 Interlayer corrugation and resistance force

3.1 Sliding of a short outer shell along a long inner tube

Consider a short outer tube sliding along the axial direction of a long inner tube. The tube lengths are taken to be $L_o \approx 36\text{\AA}$ and $L_c \approx 86\text{\AA}$. The variation of interlayer potential energy as a function of the sliding displacement is plotted in Fig. 1 for the armchair/armchair (1/1), zigzag/zigzag (0/0) and zigzag/armchair (0/1) bi-tube systems with $R_c \cong 20\text{\AA}$.

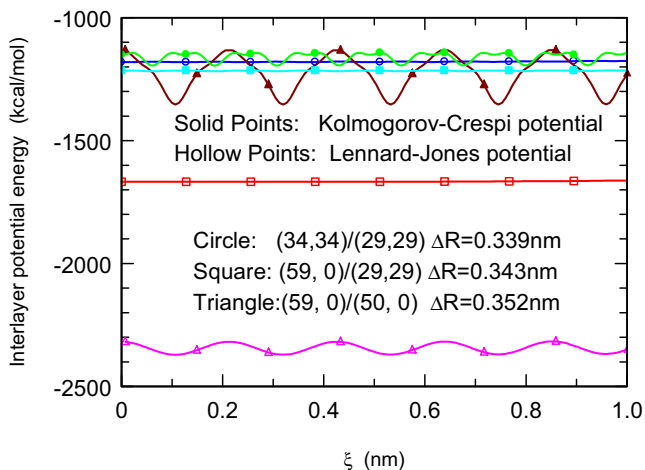


Figure 1 : Variation of interlayer potential energy with sliding displacement in a bi-tube system.

We define the interlayer corrugation as the maximal variation in the total interlayer potential energy as the outer tube slides over a whole unit cell of the inner tube or rotates over a whole circle with respect to the inner tube. It can be seen from Fig. 1 that the K-C corrugation is much more sensitive to x_o/x_c than the L-J corrugation. The main reason may be that the L-J potential is only dependent on the inter-atom distance, while the K-C potential depends not only on the inter-atom distance, but also on the interlayer space as well as the transverse separation. The sliding corrugation is lowest in the 0/1 system and highest in the 0/0 system. The L-J potential shows the effect of registry dependent corrugation, although this effect is weaker than that associated with the K-C potential. The average value of the L-J interlayer potential energy is sensitive to the interlayer distance. In comparison, the K-C potential energy changes only slightly with

the interlayer distance. When ΔR is too small, the L-J interlayer potential energy even becomes positive so that the system is unstable, but the K-C energy still remains close to that of $\Delta R \approx 3.4\text{\AA}$.

The interlayer sliding resistance force is more sensitive to the registry between the outer and inner tubes, as shown by Fig. 2. Both K-C and L-J potentials show that the fluctuation of resistance force has a discrepancy of two orders in magnitude among the 1/1, 0/1 and 0/0 bi-tube systems. The force fluctuation may lead directly to energy dissipation so that it is an important index for interlayer friction. The force fluctuation in the 0/1 bi-tube system is the lowest, with magnitude of 0.01 and 0.31 pN/atom for the L-J and K-C potentials, respectively. In contrast, the force fluctuation in the 0/0 bi-tube system is the highest, reaching as high as 2.8 and 14 pN/atom for the L-J and K-C potentials, respectively. As an example of the intermediate cases, the force fluctuation in the 1/1 system is calculated to be 0.2 and 8.1 pN/atom for the L-J and K-C potentials, respectively. The smallest interlayer force fluctuation is similar to that estimated by Cumings and Zettl (2000).

From Fig. 3 and comparison of Fig. 3 with Fig. 2, it can be found that the sliding corrugation and resistance force per atom in the 1/1 and 0/0 systems varies slightly with the tube radius but are independent of the tube length. The maximum of resistance force of the L-J potential is $f_{L-J} \approx 2.4$ pN/atom for (18,0)/(9,0) and 0.16 pN/atom for (10,10)/(5,5), and that of the K-C potential is $f_{K-C} \approx 13$ pN/atom for (18,0)/(9,0) and 2 pN/atom for (10,10)/(5,5) tube systems.

In the 0/1 tube system, however, the corrugation and resistance force are dependent on both the tube radius and tube length. The maximum resistance force of a (18,0)/(5,5) system is plotted in Fig. 4. It is seen that both f_{K-C} and f_{L-J} change with the number of atoms, although f_{L-J} is nearly two orders of magnitude lower than f_{K-C} . In our range of investigation, the forces decrease with the number of atoms in the outer shell.

3.2 Interlayer rotating resistance

The rotation corrugation and fluctuation of resistance force in 1/1, 0/0 and 0/1 bi-tube systems are extremely low, on the order of $10^{-17} \sim 10^{-18}$ N/atom, by both L-J and K-C potentials. In 1/1 and 0/0 systems, the maximum resistance force per atom is independent of the number of atoms and there is a slight dependence in the

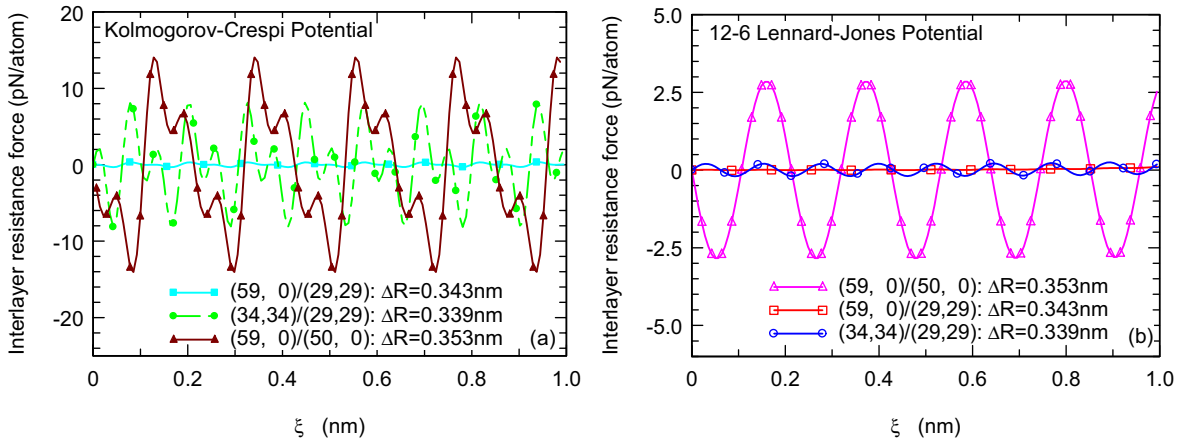


Figure 2 : Interlayer sliding resistance force associated with (a) the K-C potential and (b) the L-J potential.

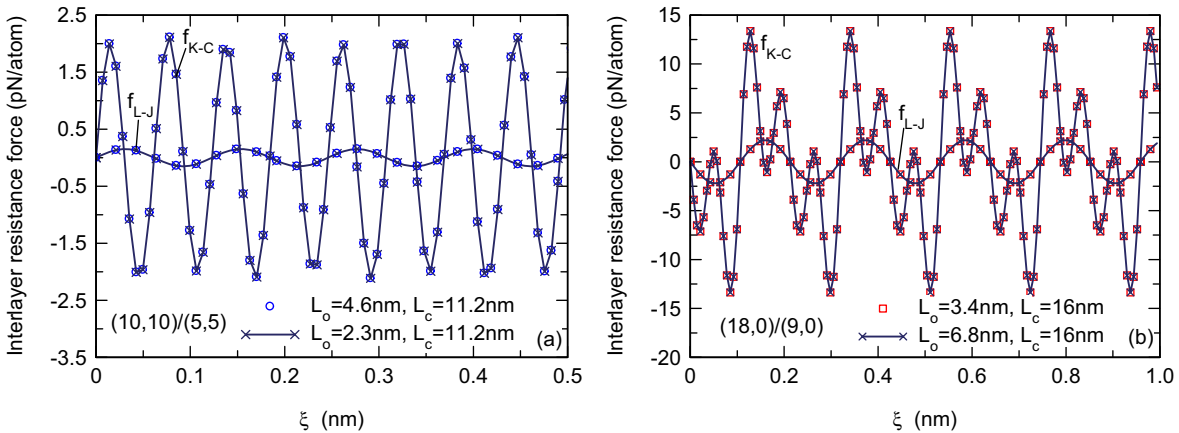


Figure 3 : Tube length effects on the interlayer sliding resistance force from both K-C and L-J potentials in (a) 1/1 and (b) 0/0 systems with $R_c \cong 3.39\text{\AA}$.

0/1 system. These systems are the smoothest rotational bearings. In systems with arbitrary x_o/x_c , fluctuation of the rotational resistance can be several orders of magnitude higher and also depends on the size of the system. Typical result is shown in Fig. 5.

The results of sliding and rotating resistance forces for bi-tube systems with $R_c \approx 20\text{\AA}$ are listed in Tab. 1. In the cases of sliding, the number of atoms is about 2000 in the outer shell, and 4000 in the inner shell. The results are obtained by sliding the outer tube along the middle portion of the inner tube. In the case of rotation, $L_o \approx L_c \approx 33\sim 36\text{\AA}$. The maximum sliding resistance forces of the 1/1 and 0/0 systems are one to two orders of magnitude higher than those of the other systems. When the L-J potential is used, the maximum sliding resistance is highest

in the 0/0 systems, about 3×10^{-12} N/atom, and is second highest in the 1/1 system, about 2×10^{-13} N/atom, and lowest in few cases at about $0.8 \sim 2 \times 10^{-17}$ N/atom, and in the rest systems it is in the range of $10^{-15} \sim 10^{-13}$ N/atom; the maximum rotating resistance is about 10^{-17} N/atom in the 1/1, 0/1 and 0/0 systems and in the range of $0.4 \times 10^{-16} \sim 0.9 \times 10^{-13}$ N/atom for the rest cases. The K-C potential leads to higher resistance forces in most of the situations except the 1/1, 0/0 and 0.4/0 systems, in which cases the maximum resistance is less than about 0.5 pN/atom. In many cases, both potentials lead to maximum resistance force on the order of 10^{-14} N/atom, and in some special cases, the force can be as low as 10^{-18} N/atom. These results provide a guide to understand the variation of resistance forces against interlayer motion in CNTs.

Table 1 : Interlayer sliding and rotating resistance forces in double walled CNTs.

Inner tube x_c (n_c, m_c)	outer tube x_o (n_o, m_o)	ΔR (Å)	f_{L-J} (pN/atom)		f_{K-C} (pN/atom)		
			sliding	rotating	sliding	rotating	
(Rc=19.9636)	0.000 (51, 0)	0.000 (60, 0)	3.5230	2.936	~0.00003	14.158	~0.000007
	0.185 (54, 10)	3.3790	0.072	0.0004	0.232	0.004	
	0.204 (54, 11)	3.6239	0.003	0.027	0.140	0.007	
	0.396 (48, 19)	3.4478	0.056	0.011	0.420	0.760	
	0.581 (43, 25)	3.3560	0.061	0.025	0.242	0.043	
	0.605 (43, 26)	3.6628	0.019	0.020	0.100	0.033	
	0.816 (38, 31)	3.4675	0.041	0.010	0.170	0.013	
	1.029 (34, 35)	3.4282	0.030	0.010	0.260	0.015	
(Rc=20.0020)	0.196 (46, 9)	0.000 (60, 0)	3.4847	~0.000008	0.010	0.009	0.086
	0.204 (54, 11)	3.5856	0.005	0.041	<u>0.110</u>	0.110	
	0.396 (48, 19)	3.4095	0.032	0.071	0.100	0.084	
	0.605 (43, 26)	3.6245	0.018	0.017	0.080	0.051	
	0.816 (38, 31)	3.4291	0.010	0.071	0.094	0.130	
	1.029 (34, 35)	3.3899	0.011	0.034	0.075	0.148	
	1.000 (35, 35)	3.7280	0.0003	0.003	0.0004	0.016	
(Rc=19.9329)	0.390 (41, 16)	0.017 (59, 1)	3.3605	0.029	0.089	0.070	0.212
	0.000 (60, 0)	3.5537	~0.000008	0.006	0.028	0.025	
	0.185 (54, 10)	3.4097	0.015	0.051	0.086	0.160	
	0.396 (48, 19)	3.4786	0.006	0.080	<u>0.055</u>	0.114	
	0.581 (43, 25)	3.3868	0.014	0.181	0.088	0.100	

(Table 1 continue)

	0.605 (43, 26)	3.6936	0.003	0.018	0.017	0.033
	0.816 (38, 31)	3.4982	0.014	0.046	0.090	0.128
	1.029 (34, 35)	3.4589	0.011	0.036	0.055	0.120
0.611 (36, 22)	0.017 (59, 1)	3.4413	0.019	0.058	0.056	0.115
	0.208 (53, 11)	3.3491	0.092	0.111	0.251	0.114
(Re= 19.8520)	0.185 (54, 10)	3.4906	0.035	0.054	0.047	0.103
	0.396 (48, 19)	3.5595	0.009	0.025	0.103	0.073
	0.619 (42, 26)	3.4117	0.032	0.128	<u>0.270</u>	0.270
	0.816 (38, 31)	3.5791	0.005	0.026	0.026	0.040
	1.029 (34, 35)	3.5398	0.021	0.049	0.070	0.092
0.844 (32, 27)	0.000 (60, 0)	3.4617	~0.00002	0.002	0.004	0.031
	0.204 (54, 11)	3.5626	~0.000008	0.114	0.117	0.144
(Re=20.0249)	0.396 (48, 19)	3.3865	0.014	0.067	0.407	0.179
	0.417 (48, 20)	3.6695	0.002	0.004	0.040	0.052
	0.605 (43, 26)	3.6015	0.005	0.025	0.050	0.121
	0.816 (38, 31)	3.4062	0.009	0.038	<u>0.207</u>	0.178
	1.029 (34, 35)	3.3669	0.040	0.087	0.159	0.154
	1.000 (35, 35)	3.7051	~0.000008	0.013	0.016	0.017
1.000 (29, 29)	0.000 (59, 0)	3.4332	0.008	~0.00001	0.310	~0.000002
	0.208 (53, 11)	3.5391	0.005	0.017	0.026	0.030
(Re=19.6620)	0.404 (47, 19)	3.3734	0.010	0.057	0.114	0.030
	0.396 (48, 19)	3.7495	0.005	0.025	0.145	0.028
	0.619 (42, 26)	3.6017	0.001	0.011	0.035	0.048

(Table 1 continue)

0.789 (38, 30)	3.4431	0.001	0.005	0.039	0.026
1.000 (34, 34)	3.3900	0.190	~ 0.00004	<u>8.100</u>	~ 0.00001
1.029 (34, 35)	3.7298	0.0002	0.007	0.004	0.010

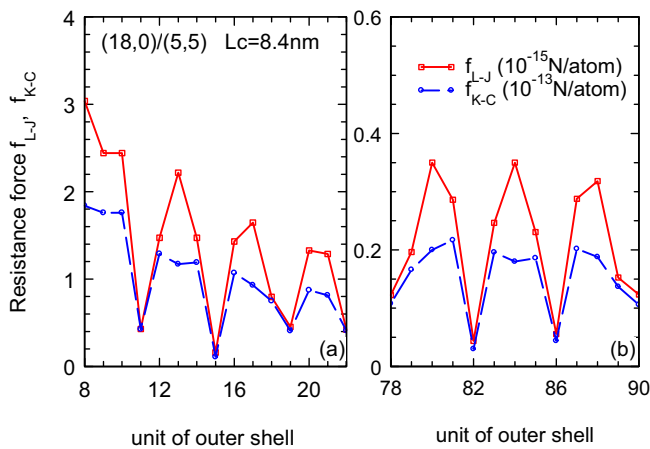


Figure 4 : The maximum sliding resistance force as a function of the number of atoms in the (18,0)/(5,5) bi-tube system.

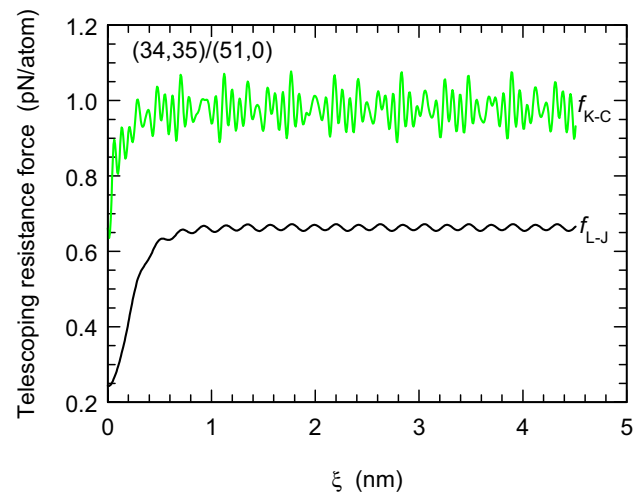


Figure 6 : Typical variation of telescoping interlayer resistance to intertube displacement.

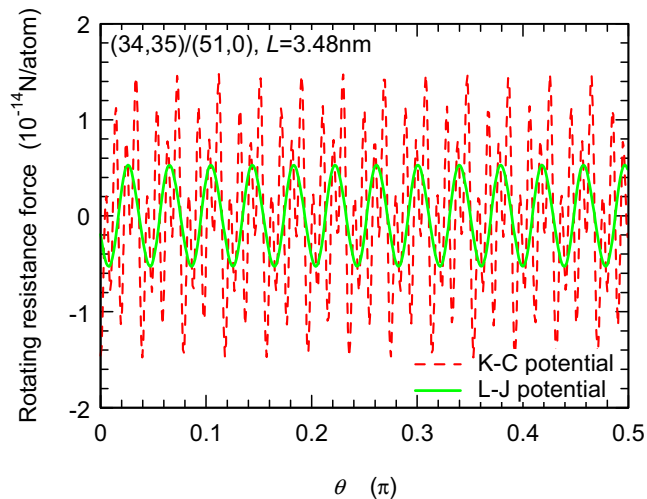


Figure 5 : Typical rotation resistance curve of an incommensurate tube system.

3.3 Telescoping resistance

An important mode of interlayer sliding is to telescope the inner tube from the outer tube. In such a situation, the number of atoms in the overlap section changes with the relative motion of the two tubes. The characteristics of this kind of telescoping resistance are quite different from the resistance to slide a short tube on a long tube. A typical variation of the telescoping interlayer resistance with respect to intertube displacement is shown in Fig. 6. In the initial stage, the force increases with telescoping length, ξ . When ξ is greater than about 0.5nm, the average resistance force (\bar{f}) tends to a steady-state value depending on x_o/x_c . This is mainly because of the relative positions of the four ends of the two shells and the built up of finite-range effects in the potentials. In the steady-state stage, the resistance force changes periodically around the average value with a maximum amplitude Δf . In most cases, Δf is nearly constant and is small

in comparison to \bar{f} . Both Δf and \bar{f} is strongly dependent on x_o/x_c . Therefore, \bar{f} and Δf play a role in the interlayer resistance.

3.3.1 Size effects

As shown in Tab. 2 where we have chosen $L = L_c \approx L_o$, the average telescoping force in the steady-state stage is independent of tube length, but the fluctuation depends not only on x_o/x_c , but also on the tube length L . Typical results for the 1/1 and 0/0 systems are shown in Fig. 7. In the 1/1 system, Δf_{L-J} is nearly in linear proportion to the number of atoms, or $\Delta f_{L-J}/N_c$ is nearly constant. In the 0/0 system, however, $\Delta f_{L-J}/N_c$ is an increasing function of length. For example, $\Delta f_{L-J}/N_c = 6.84, 7.08$ and 7.87 pN/atom for the (18,0) / (9,0) system with $L = 4.3, 8.6$ and 17.8 nm, respectively. It can also be seen that Δf_{L-J} decreases with increasing telescoping distance, or decreasing number of overlapping atoms in both 0/0 and 1/1 systems. In comparison, the Δf_{K-C} in these systems is much greater than \bar{f}_{K-C} and is generally too large to be shown in the same figure with f_{L-J} .

In the 0/1 system, the fluctuations of resistance forces Δf_{L-J} and Δf_{K-C} are independent of the tube length but they increase with the tube radius as shown by Fig. 8 and are much smaller than the corresponding values in the 1/1 and 0/0 systems. When the tube length increases, the force fluctuation per atom will decrease. For example, for (18,0)/(5,5) systems with tube lengths of 5, 20 and 100nm, $\Delta f_{L-J}/N_c = 0.016, 0.0039$ and 0.00078 pN/atom, and $\Delta f_{K-C}/N_c = 0.26, 0.066$ and 0.013 pN/atom respectively. Therefore, the 0/1 system is the smoothest pair of tubes to telescope. The average telescoping force does not change with tube length, but changes with tube radius.

Further study on the size effect in more general cases shows that for $x_c = x_o$, both Δf_{L-J} and Δf_{K-C} increase with tube length and are nearly proportional to the number of atoms. For axial incommensurate systems with $x_c \neq x_o$, Δf_{L-J} and Δf_{K-C} do not change with tube length and the resistance per atom decreases with increasing tube length and can be extremely low for long tube systems. Fig. 9 shows the results for x_o/x_c other than 0/1. Our studies also show that the fluctuation of resistance force depends on the tube radius, as illustrated in the last three rows of Tab. 2. In most cases, the force fluctuation increases with increasing tube radius. However, changes in tube radius usually induce only moderate variation in

the fluctuation of resistance forces without altering their order of magnitude.

In Tab. 3, the telescoping forces for bi-tube systems with x_o and $x_c \cong 0, 0.2, 0.4, 0.6, 0.8$ and 1.0 are listed for $R_c \approx 2$ nm. The tube combinations are chosen to have interlayer gap nearest to 0.34 nm while greater than 0.339 nm for the required x_o/x_c . The length of the tube is about 3.4 nm with $N_o \cong 2000$ and $N_c \cong 1600$, and the forces are divided by N_o in the table. The average \bar{f} and fluctuation range Δf of the telescoping force is taken from the steady-state stage. Here, Δf is the difference between the maximum and minimum values over the whole steady-state stage and $f_{max} = \bar{f} + \Delta f/2$ stands for the maximum telescoping resistance and Δf is closely related to the interlayer friction force.

We find that for given x_c , the L-J interlayer telescoping force \bar{f}_{L-J} is the lowest when the interlayer gap ΔR is nearest to 0.34 nm (as shown by underline), which happens at $x_o \cong x_c$ when $x_c \geq 0.6$. However, Δf_{L-J} in such a tube pair is not the lowest. In contrast, Δf_{L-J} is largest at $x_o = x_c = 1$ and 0 , and Δf_{K-C} is largest for all $x_o = x_c$ except for $x_c \cong 0.4$. The K-C potential is not sensitive to ΔR and the smallest \bar{f}_{K-C} has no significant relation with x_o/x_c or ΔR . This phenomenon may implicate that the L-J potential can provide rather reasonable prediction dependency of the interaction upon the interlayer distance. As both potentials are empirical ones, more subtle details need further study.

Except for the cases of $x_o = x_c = 1$ and 0 , Δf_{L-J} varies in the range between 8×10^{-14} N/atom and 3.2×10^{-16} N/atom; Δf_{K-C} varies in a much smaller range of 1.5 to 80×10^{-14} N/atom. In the case with ΔR is not smaller than but close to 0.34 nm for a given x_c , Δf_{L-J} only changes from 0.72 to 1.75×10^{-14} N/atom. For the lowest \bar{f}_{K-C} under fixed x_c , Δf_{K-C} is limited to 1.1 to 10.9×10^{-14} N/atom. If we define the static telescoping friction force by $f_i = \Delta f/2$, it can be concluded that, at least for the size used in Tab. 3, the friction force is on the order of $0.36 \sim 5 \times 10^{-14}$ N/atom in the optimized cases.

3.3.2 Mixed telescoping and rotating

Mixed telescoping and rotation can be characterized by the factor $\beta = R_c \theta / \xi$. For the 0/0 and 1/1 systems, change of β has only very slight effect on the telescoping force f_{L-J} , but has strong effect on rotating force f_{L-J} . The effect of β on the force f_{K-C} is very significant for both rotation and telescoping. For the 0/1 system, however,

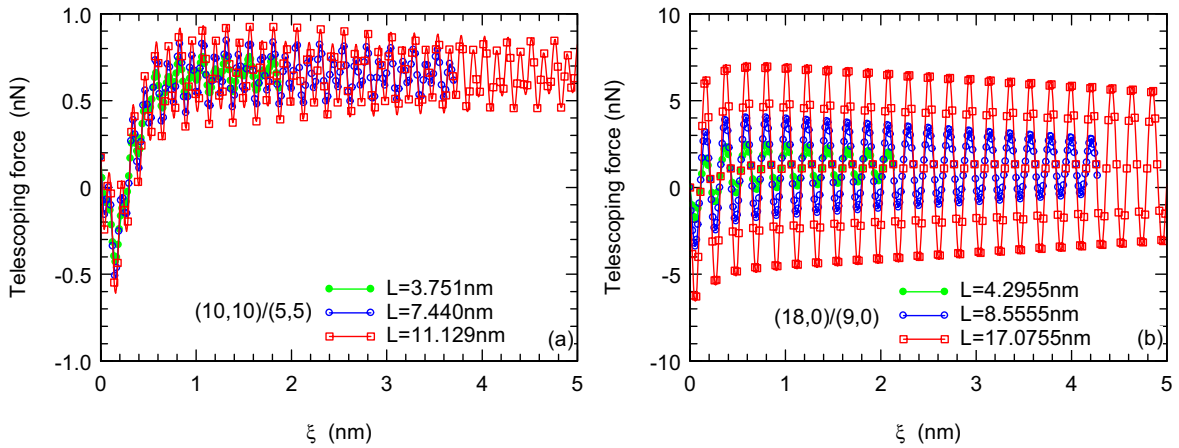


Figure 7 : Variation of telescoping resistance forces in commensurate (a) 1/1 and (b) 0/0 systems.

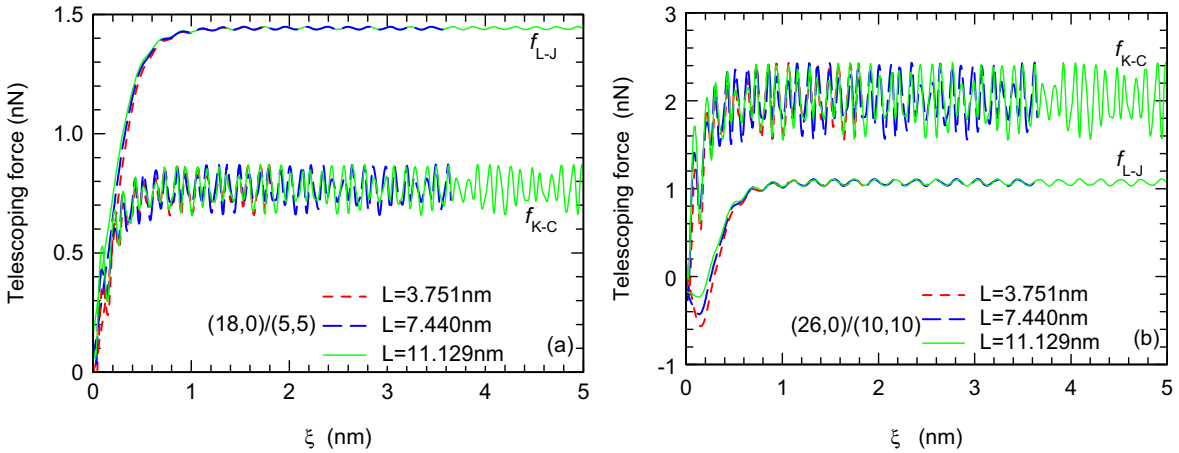


Figure 8 : The length independent fluctuation of telescoping force in 0/1 systems with (a) small and (b) large radii.

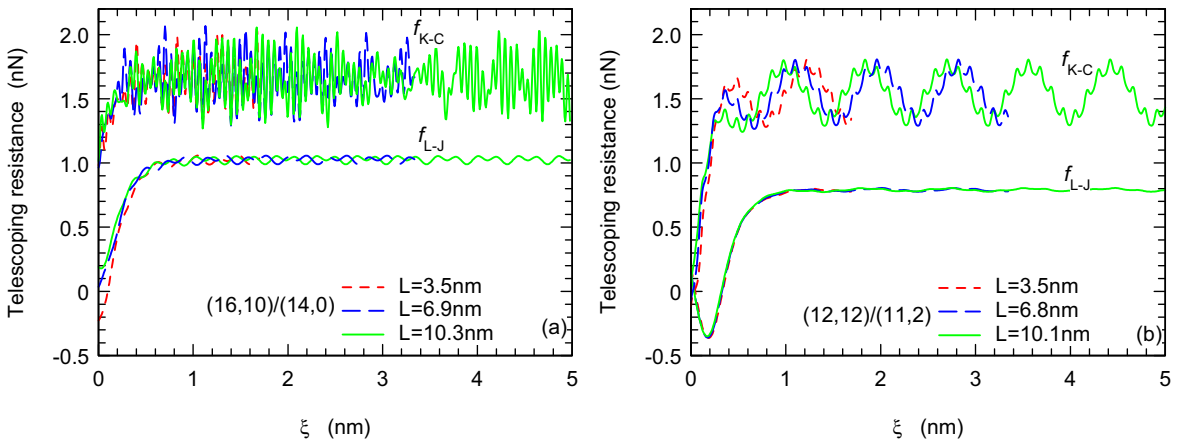


Figure 9 : The effect of tube length on the telescoping force in incommensurate tube systems: (a) 0.625/0 and (b) 1/0.182 systems.

Table 2 : Effects of nanotube sizes on the telescoping interlayer resistance force.

Tube system	N_c	L_c	\bar{f}_{L-J}	Δf_{L-J}	$\Delta f_{L-J}/N_c$	\bar{f}_{K-C}	Δf_{K-C}	$\Delta f_{K-C}/N_c$
ΔR (nm)		(nm)	(pN)	(pN)	(pN/atom)	(pN)	(pN)	(pN/atom)
	300	3.751		208	0.69		3550	11.90
(10,10)/(5,5)	600	7.440	656	391	0.65	1250	5010	8.40
0.3390	900	11.129		587	0.65		8450	9.40
	360	4.296		2451	6.84		17739	49.30
(18,0)/(9,0)	720	8.556	1156	5114	7.08	900	37037	51.40
0.3523	1440	17.755		11349	7.87		75634	52.50
	300	3.751			0.04			0.73
(18,0)/(5,5)	600	7.440	1442	13	0.02	772	218	0.36
0.3656	900	11.129			0.01			0.24
	600	3.751			0.13			14.70
(26,0)/(10,10)	1200	7.440	1071	81	0.07	202	88	0.07
0.3398	1800	11.129			0.04			0.05
(59,0)/(29,29)	1740	3.751	3364	171	0.10	478	190	0.11
0.3433	3480	7.440			0.05			0.06

the telescoping force f_{L-J} and rotating force f_{L-J} are independent of β .

4 Intralayer deformation effects

It has already been shown¹ that, since the in-plane modulus is much higher comparing to the weak interlayer interaction, the effect of deformation is only moderate and will not change the general trends obtained above. Fig. 10 shows the comparison between results from rigid tubes and results of quasi-static MD. In the quasi-static MD simulation, the Tersoff-Brenner potential is used and the core tube is telescoped out of the outer tube step by

step just like in the above theoretical analysis, but the tube system is relaxed at the beginning and at every step in the simulation. The discrepancy caused by the deformation of tubes is relatively small in both of the tube system shown in Fig. 10.

5 Molecular dynamics simulations

Molecular dynamics (MD) simulations are performed on the (10,10)/(5,5), (18,0)/(5,5) and (18,0)/(9,0) oscillating systems with length $L \approx 3.4$ nm. The inner core tube is telescoped out to about $1/4L$ and the system is relaxed to its minimum energy state with the outer shell being fixed

Table 3 : Interlayer telescoping resistance force in double walled CNTs.

Inner tube		outer tube	ΔR	f_{L-J} (pN/atom)		f_{K-C} (pN/atom)		
x_c	(n_c, m_c)	x_o	(n_o, m_o)	(\AA)	Δf_{L-J}	\bar{f}_{L-J}	Δf_{K-C}	\bar{f}_{K-C}
0.000	(51, 0)	0.000	(60, 0)	3.5230 ^a	1.988	0.997	6.793	1.335
		0.204	(54, 11)	3.6239	0.014	1.171	0.063	<u>0.703</u> ^b
		0.396	(48, 19)	3.4478	0.028	0.747	0.767	0.938
		0.605	(43, 26)	3.6628	0.027	1.202	0.015	1.512
		0.816	(38, 31)	3.4675	0.019	0.817	0.070	0.915
		1.029	(34, 35)	3.4282	0.018	<u>0.670</u> ^b	0.188	0.975
0.196	(46, 9)	0.000	(60, 0)	3.4847	0.027	0.907	0.124	0.905
		0.204	(54, 11)	3.5856 ^a	0.005	1.1100	0.189	0.733
		0.396	(48, 19)	3.4095	0.015	<u>0.586</u> ^b	0.104	1.019
		0.605	(43, 26)	3.6245	0.009	1.171	0.058	0.694
		0.816	(38, 31)	3.4291	0.006	0.672	0.073	0.981
		1.029	(34, 35)	3.3899	0.001	1.295	0.011	<u>0.615</u> ^b
0.390	(41, 16)	0.000	(60, 0)	3.5537	0.021	1.077	0.091	0.819
		0.185	(54, 10)	3.4097	0.014	<u>0.606</u> ^b	0.075	1.053
		0.396	(48, 19)	3.4786 ^a	0.010	0.843	0.061	0.885
		0.605	(43, 26)	3.6936	0.002	1.229	0.030	<u>0.628</u> ^b
		0.816	(38, 31)	3.4982	0.007	0.899	0.060	0.852
		1.029	(34, 35)	3.4589	0.004	0.778	0.092	0.921
0.611	(36, 22)	0.017	(59, 1)	3.4413	0.010	0.711	0.062	0.951
		0.185	(54, 10)	3.4906	0.007	0.913	0.144	0.902
		0.396	(48, 19)	3.5595	0.004	1.043	0.043	0.760

(Table 3 continue)

	0.619 (42, 26)	3.4117 ^a	0.015	<u>0.612</u> ^b	0.298	1.039
	0.816 (38, 31)	3.5791	0.001	1.080	0.019	<u>0.740</u> ^b
	1.029 (34, 35)	3.5398	0.007	1.002	0.042	0.797
0.844 (32, 27)	0.000 (60, 0)	3.4617	0.018	0.824	0.080	0.971
	0.204 (54, 11)	3.5626	0.008	1.061	0.107	0.770
(Rc=20.0249)	0.417 (48, 20)	3.6695	0.003	1.263	0.039	0.679
	0.605 (43, 26)	3.6015	0.003	1.130	0.032	0.721
	0.816 (38, 31)	3.4062 ^a	0.007	<u>0.570</u> ^b	0.355	1.026
	1.000 (35, 35)	3.7051	0.001	1.268	0.023	<u>0.646</u> ^b
1.000 (29, 29)	0.000 (59, 0)	3.4332	0.037	0.712	0.417	1.006
	0.208 (53, 11)	3.5391	0.002	0.992	0.022	0.786
(Rc=19.6620)	0.396 (48, 19)	3.7495	0.003	1.263	0.109	<u>0.575</u> ^b
	0.619 (42, 26)	3.6017	0.0003	1.157	0.092	0.740
	0.789 (38, 30)	3.4431	0.0006	0.740	0.029	0.977
	1.000 (34, 34)	3.3900 ^a	0.356	<u>0.509</u> ^b	15.945	1.123

^a for $x_o \cong x_c$. ^b for the smallest telescoping force. $N_o \cong 2000$, $N_c \cong 1600$.

by two atoms at one end and one atom at another end to remove the rigid movement of the outer tube. Both inner and outer tubes are free-open ended. Then the core is released and begins to oscillate with respect to the outer shell driven by the van der Waals force of the interlayer L-J interaction. This is simulated using molecular dynamics at an initial temperature of 8K with constant total energy control. The intra-shell atomic interactions are modeled by the standard AMBER molecular force field. The time step is 1fs in the simulation which is much smaller than the period of oscillation (about 10ps) and the simulating duration is up to order of nanoseconds to show the clear trend for comparison. The details of the simulations are the same as in [Guo, Guo, Gao, Zheng

and Zhong (2003)].

Once the core is released, it will retract into the outer shell under the interlayer interaction and the potential energy will decrease while the kinetic energy increases. When the core is completely retracted into the outer shell, the interlayer potential energy decreases to its minimum value but the core has accelerated to its maximum speed. Under the action of inert force, the core moves out of the outer shell in the opposite end, forming a nano-oscillator [Zheng and Jiang (2002)]. The fluctuation of the interlayer resistance causes energy dissipation so that the oscillating amplitude decreases with time [Guo, Guo, Gao, Zheng and Zhong (2003); Rivera, McCabe and Cummings (2003)]. This oscillator system is used to demon-

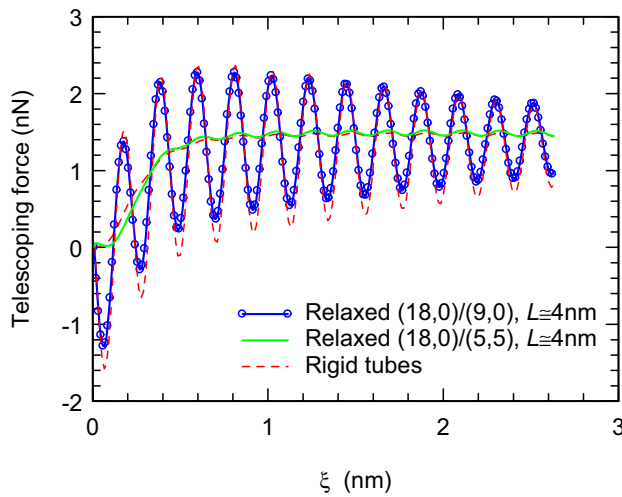


Figure 10 : The influence of tube deformation on the interlayer telescoping force in both 0/0 and 0/1 systems.

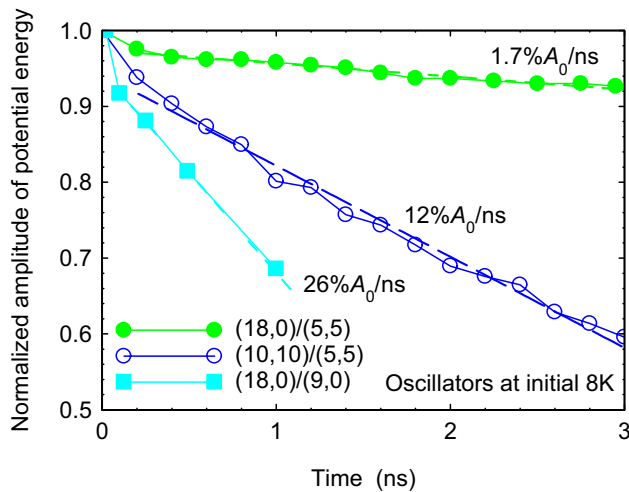


Figure 11 : Dissipation rate of potential energy in the 0/1, 1/1 and 0/0 bi-tube oscillators. The amplitude of the potential energy is normalized by its value A_0 at beginning of oscillating, which is about 70kcal/mol in the MD simulations.

strate the orientation dependent fluctuation of interlayer resistance forces calculated in this paper. The results plotted in Fig. 11 show that the rate of energy dissipation rate is much slower in the (18,0)/(5,5) system than in the (10,10)/(5,5) system, and the dissipation rate in the (18,0)/(9,0) system is the highest, where the amplitude of the potential energy is normalized by its value A_0 at the beginning of oscillation. In the present simulations,

A_0 is about 69 to 73kcal/mol. The energy dissipation rate of the three system are 1.7%, 12% and 26% A_0 per nanosecond. The predicted durations of sustained oscillation from the figure are about 58, 8 and 4ns for the three cases. The effective dynamic interlayer friction forces as defined in [Guo, Guo, Gao, Zheng and Zhong (2003)] for the three cases are 0.085, 0.400 and 0.612pN/atom respectively. In comparison, the static force fluctuations of the systems are about 0.04, 0.07 and 7.0 pN/atom. Therefore the general trend of registration dependence of the interlayer friction is the same from both molecular statics and dynamics, but the static force fluctuation is not in proportional to the dynamic friction force. Both static and dynamic results show that the 0/1 system is smoother than the 1/1 system and the 0/0 system is the toughest. In the constant total energy control systems, losses in mechanical potential and kinetic energies change into thermal energy and cause rise in temperature. The 0/1 and 1/1 systems have increments of about 1.2K and 6K in the 3ns simulation respectively, while the increment in the 0/0 system in 1ns is as high as 6.6K. Extended research on effects of many other factors, such as defects, size and terminal conditions of the tubes systems on the energy dissipation will be studied in a separate paper.

6 Conclusions

Systematic investigations of sliding, rotation and telescoping interlayer interaction between any two possible neighboring carbon nanotubes are performed in the present work theoretically. The interlayer corrugation energy and the details of the variation of the interlayer resistance force for sliding, rotation, telescoping and coupled telescoping and rotation between any possible bi-tube systems are analyzed by assuming that the interlayer interaction is characterized by either the classical Lennard-Jones (L-J) potential or a registry-dependent graphitic potential (K-C potential). It is found that the energy dissipation related fluctuation of interlayer interaction forces can vary significantly with the morphology, length and diameter of the two tubes. The dependence of the force fluctuation upon the registry and size of the bi-tube systems are quite different in the three modes of interlayer motion. For a short outer shell sliding along a long inner tube core, the maximum interlayer resistance force of an axially commensurate system is independent of the length of the outer tube and can be one to two orders of magnitude higher than those of the other systems.

When the L-J potential is used, the maximum fluctuation of the sliding force are in the range of $10^{-17} \sim 10^{-12}$ N/atom, while the K-C potential predicts a much higher fluctuation. The rotation corrugation and force fluctuation in systems with any combination of zigzag and/or armchair tubes are extremely low, usually on the order of $10^{-17} \sim 10^{-18}$ N/atom, according to both L-J and K-C potentials. These systems are the smoothest rotational bearings. In comparison, fluctuation of the rotational resistance in systems with arbitrary registry can be several orders of magnitude higher and depend strongly on the size of the system.

In case of telescoping a core tube out of an outer shell in commensurate systems, the fluctuations of the interlayer forces given by both L-J and K-C potentials increase with the tube length and are nearly proportional to the number of atoms. For axial incommensurate systems, the force fluctuation given by both potentials is found to be independent of the tube length and vary in the range of 8×10^{-14} N/atom to 3.2×10^{-16} N/atom for the L-J potential and in the range of 1.5 to 80×10^{-14} N/atom for the K-C potential. This means that the force fluctuation per atom in an incommensurate system decreases with increasing tube length and the telescoping friction force per atom can be reduced by increasing the tube length. The rotational motion has only slight influence on the fluctuation of telescoping force in a commensurate system, but can have significant effect in most incommensurate systems. We find that in a zigzag/armchair system, the fluctuations of both telescoping force and rotating force are independent of the mode mixity ratio so that mixed telescoping and rotating motion is most favorable to occur in this system.

The L-J potential is registry sensitive and in many cases it yields similar tendency as the K-C potential, but it is much simpler and easier to use.

Acknowledgement: We gratefully acknowledge the support of the Chinese National Natural Science Foundation. The work is also supported via a 3 month visiting professorship for WG from the Max Planck Institute for Metals Research in Stuttgart, Germany.

References

Benedict, L. X.; Chopra, N. G.; Cohen, M. L.; Zettl, A.; Louie, S. G.; Crespi, V. H. (1998): Microscopic de-

termination of the interlayer binding energy in graphite. *Chem. Phys. Lett.*, vol. 286, pp. 490-496.

Brenner, D. W.; Shenderova, O. A.; Areshkin, D. A.; Schall, J. D.; Frankland, S.-J. V. (2002): Atomic Modeling of Carbon-Based Nanostructures as a Tool for Developing New Materials and Technologies, *CMES: Computer Modeling in Engineering & Sciences*, vol. 3, no. 5, pp. 643-674.

Collins, P. G.; Arnold, M. S.; Avouris, P. (2001): Engineering Carbon Nanotubes and Nanotube Circuits Using Electrical Breakdown. *Science*, vol. 292, pp. 706-709.

Cummings, J.; Zettl, A. (2000): Low-Friction Nanoscale Linear Bearing Realized from Multiwall Carbon Nanotubes. *Science*, vol. 289, pp. 602-604.

Dai, H. (2002): Carbon nanotubes: opportunities and challenges. *Surface Sci.*, vol. 500, pp. 218-241.

Dai, H.; Wong, E. W.; Lieber, C. M. (1996): Probing Electrical Transport in Nanomaterials: Conductivity of Individual Carbon Nanotubes. *Science*, vol. 272, pp. 523-526.

Damjanovic, M.; Milosevic, I.; Vukovic, T.; Sredanovic, R. (1999): Full symmetry, optical activity, and potentials of single-wall and multiwall nanotubes. *Phys. Rev. B*, vol. 60, pp. 2728-2739.

de Heer, W. A.; Bacsá, W. S.; Chatelain, A.; Gerfin, T.; Humphrey-Baker, R.; Forro, L.; Ugarte, D. (1995): Aligned Carbon Nanotube Films: Production and Optical and Electronic Properties. *Science*, vol. 268, pp. 845-847.

Forro, L. (1995): NANOTECHNOLOGY: Beyond Gedanken Experiments. *Science*, vol. 289, pp. 560-561.

Girifalco, L. A.; Hodak, M. (2002): Van der Waals binding energies in graphitic structures. *Phys. Rev. B*, vol. 65, pp. 125404.

Guo, W.; Guo, Y.; Gao, H.; Zheng, Q.; Zhong, W. (2003): Energy Dissipation in Gigahertz Oscillators from Multiwalled Carbon Nanotubes. *Phys Rev Lett*, vol. 91, pp. 125501.

Guo, Y.; Guo, W. (2003): Mechanical and electrostatic properties of carbon nanotubes under tensile loading and electric field. *J. Phys. D: Appl. Phys.*, vol. 36, pp. 805-811.

Hamada, N.; Sawada, S.; Oshiyama, A. (1992): New one-dimensional conductors: Graphitic microtubules. *Phys. Rev. Lett.*, vol. 68, pp. 1579-1581.

- Hirano, M.; Shinjo, K.; Kaneko, R.; Murata, Y.** (1997): Observation of Superlubricity by Scanning Tunneling Microscopy. *Physical Review Letters*, vol. 78, pp. 1448-1451.
- Kolmogorov, A. N.; Crespi V. H.** (2000): Smoothest bearings: interlayer sliding in multiwalled carbon nanotubes. *Phys. Rev. Lett.*, vol. 85, pp. 4727 - 4730.
- Legoas, S. B.; Coluci, V. R.; Braga, S. F.; Coura, P. Z.; Dantas, S. O.; Galvao, D. S.** (2003): Molecular-Dynamics Simulations of Carbon Nanotubes as Gigahertz Oscillators. *Phys Rev Lett*, vol. 90, pp. 055504.
- Martel, R.; Schmidt, T.; Shea, H. R.; Hertel, T.; Avouris, P** (1998): Single- and multi-wall carbon nanotube field-effect transistors. *Appl. Phys. Lett.*, vol. 73, pp. 2447-2449.
- Odom, T. W.; Huang, J.-L.; Kim, P.; Lieber, C. M.** (1998): Atomic structure and electronic properties of single-walled carbon nanotubes. *Nature* (London), vol. 391, pp. 62-64.
- Paulson, S.; Helser, A.; Nardelli, M.; Taylor II, R. M.; Falvo, M.; Superfine, R.; Washburn, S.** (2000): Tunable Resistance of a Carbon Nanotube-Graphite Interface. *Science*, vol. 290, pp. 1742-1744.
- Postma, H. W.; Teepen, T.; Yao, Z.; Grifoni, M.; Dekker, C.** (2001): Carbon Nanotube Single-Electron Transistors at Room Temperature. *Science*, vol. 293, pp. 76-79.
- Rivera, J. L.; McCabe, C.; Cummings, P. T.** (2003): Oscillatory Behavior of Double-Walled Nanotubes under Extension: A Simple Nanoscale Damped Spring. *Nano Lett*, vol. 3, pp. 1001-1005.
- Robertson, D. H.; Brenner, D. W.; Mintmire, J. W.** (1992): Energetics of nanoscale graphitic tubules. *Phys.Rev. B*, vol. 45, pp. 12592-12595.
- Roche, S.; Triozon, F.; Rubio, A.; Mayou, D.** (2001): Electronic conduction in multi-walled carbon nanotubes: role of intershell coupling and incommensurability. *Phys. Lett. A*, vol. 285, pp. 94-100.
- Rueckes, T.; Kim, K.; Joselevich, E.; Tseng, G. Y.; Cheung, C.-L.; Lieber, C. M.** (2000): Carbon Nanotube-Based Nonvolatile Random Access Memory for Molecular Computing *Science*, vol. 289, pp. 94-97.
- Shyu, F. L.; Lin, M. F.** (2000): Loss spectra of graphite-related systems: A multiwall carbon nanotube, a single-wall carbon nanotube bundle, and graphite layers. *Phys. Rev. B*, vol. 62, pp. 8508-8516.
- Shen, S. P.; Atluri, S. N.** (2004): Multiscale Simulation Based on The Meshless Local Petrov-Galerkin (MLPG) Method, *CMES: Computer Modeling in Engineering & Sciences*, vol. 5, no. 3, pp. 235-256.
- Tanaka, K.; Aoki, H.; Ago, H.; Yamare, T.; Okahara, K.** (1997): Interlayer interaction of two graphene sheets as a model of double-layer carbon nanotubes. *Carbon*, vol. 35, pp. 121-125.
- Tans, S. J.; Verschueren, A. R. M.; Dekker, C.** (1998): Room-temperature transistor based on a single carbon nanotube. *Nature* (London), vol. 393, pp. 49-52.
- Treacy, M. M.; Ebbesen, T. W.; Gibson, J. M.** (1996): Exceptionally high Young's modulus observed for individual carbon nanotubes. *Nature* (London), vol. 381, pp. 678-680.
- White, C. T.; Robertson, D. H.; Mintmire, J. W.** (1993): Helical and rotational symmetries of nanoscale graphitic tubules. *Phys. Rev. B*, vol. 47, pp. 5485-5488.
- Wong, E.; Sheehan, P.; Lieber, C.** (1997): Nanobeam Mechanics: Elasticity, Strength, and Toughness of Nanorods and Nanotubes. *Science*, vol. 277, pp. 1971-1975.
- Yu, M.-F.; Lourie, O.; Dyer, M. J.; Moloni, K.; Kelly, T. F.; Ruoff, R. S.** (2000): Strength and Breaking Mechanism of Multiwalled Carbon Nanotubes Under Tensile Load. *Science*, vol. 287, pp. 637-640.
- Yu, M.-F.; Yakobson, B. I.; Ruoff, R. S.** (2000): Controlled Sliding and Pullout of Nested Shells in Individual Multiwalled Carbon Nanotubes. *J. Phys. Chem. B*, vol. 104, pp. 8764-8767.
- Zheng, Q.; Liu, J. Z.; Jiang, Q.** (2002): Excess van der Waals interaction energy of a multiwalled carbon nanotube with an extruded core and the induced core oscillation. *Physical Review B*, vol. 65, pp. 245409.
- Zheng, Q.; Jiang, Q.** (2002): Multiwalled Carbon Nanotubes as Gigahertz Oscillators. *Phys. Rev. Lett.*, vol. 88, pp. 045503.

Appendix

In this study, the interlayer interaction has been modeled with the 12-6 Lennard-Jones potential

$$V_{LJ}(r_{ij}) = 4\epsilon \left[\left(\frac{\sigma}{r_{ij}} \right)^{12} - \left(\frac{\sigma}{r_{ij}} \right)^6 \right] \quad (\text{A1})$$

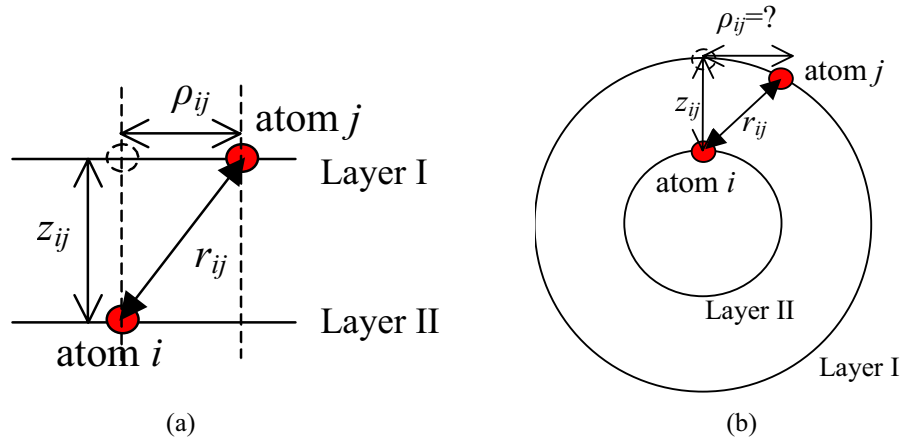


Figure A1: The variables in KC and LJ potential (a) for planar graphite bi-layers; (b) for bi-walled carbon nanotubes.

and the registry-dependent two-body graphitic potential developed by Kolmogorov and Crespi¹:

$$V_{KC}(r_{ij}) = -\left(\frac{d}{r_{ij}}\right)^6 + e^{-\lambda_1(r_{ij}-r_0)} + e^{-\lambda_2(z_{ij}-z_0)} e^{-(\rho_{ij}/\delta)^2} \sum_{n=0}^6 C_{2n} (\rho_{ij}/\delta)^{2n} \quad (\text{A2})$$

Where z is the interlayer space and ρ is the transverse separation. The constants for carbon nanotubes are as follows:

$$\varepsilon = 0.3496 \text{ kJ/mol}, \sigma = 3.851 \text{ \AA}.$$

$$C_0 = 11.964, C_2 = 6.78, C_4 = -18.418, C_6 = 9.836, C_8 = -1.8938, C_{10} = -0.6391, C_{12} = 0.08652.$$

$$d = 4.68 \text{ \AA}, r_0 = 4.00 \text{ \AA}, z_0 = 3.44 \text{ \AA}, \delta = 0.568 \text{ \AA}, \lambda_1 = 4.19 \text{ \AA}^{-1}, \lambda_2 = 3.444 \text{ \AA}^{-2}.$$

In situation of atoms in planar graphite bi-layers, as shown by Fig.A1 (a), the LJ potential only considers the distance r_{ij} between the two atoms i and j , while in the KC potential, except r_{ij} the layer gap z_{ij} , the transverse separation ρ_{ij} are included as variables as well to “reflect the registry-dependence” in two-body graphitic systems.

For atoms on two planar layers, $\rho_{ij} = \sqrt{r_{ij}^2 - z_{ij}^2}$.

When applied the KC potential to a bi-walled nanotube system as shown by Fig.A1 (b), the definition of the transverse separation ρ_{ij} becomes confusion and we use $\rho_{ij} = \sqrt{r_{ij}^2 - z_{ij}^2}$ approximately in this study.